



## **Microfluidics:**

Section Editors Dr Rashid Bashir and Dr Steve Wereley

### *Measurement of AC Electrokinetic Flows*

*Carl Meinhart,\* Dazhi Wang, and Kimberly Turner*

*E-mail: meinhart@engineering.ucsb.edu*

*Department of Mechanical and Environmental Engineering,  
Santa Barbara, California, 93106, USA*

**Abstract.** Micron-resolution particle image velocimetry ( $\mu$ -PIV) is used to measure the motion of nominally 1- $\mu$ m dia. polystyrene particles suspended in a water/sugar solution in a microdevice. Particle motion is induced by an applied electric field through dielectrophoretic (DEP) forces and through viscous interactions with the fluid. The motion of the fluid is governed by electrothermal forces arising from temperature-induced gradients in the electrical properties of the fluid near the electrodes and through the viscous interaction with the particles. Comparisons between finite element calculations and experimental micro-PIV results confirm quantitatively that electrothermal forces play a major role in the motion of the particles. Two different size particles are used for the micro-PIV measurements to determine fluid velocity uniquely.

**Key Words.** micron-resolution PIV, microfluidics, dielectrophoresis, electrothermal effect

#### **1. Introduction**

The small length scales associated with microfluidic devices provide an environment for molecular diagnostic sensors that are capable of detecting the presence of small numbers of molecules. In many cases, it is desirable to manipulate particle movement inside the device. Ac electrokinetics refers to induced particle and/or fluid motion resulting from externally applied ac electric fields. Ac electrokinetics can be classified into three broad areas: dielectrophoresis (DEP), electrothermal effects and ac electro-osmosis (Ramos et al., 1998).

Dielectrophoresis is a force applied to a particle in the presence of a non-uniform electric field. This force results from differences in polarizability between the particle and the fluid medium.

Electrothermal body forces result from spatial variations in electric field, creating non-uniform Joule heating of the medium. The Joule heating is a source term in the temperature equation, and creates spatial variations in conductivity and permittivity, which in turn create Coulomb and dielectric body forces in the

presence of an externally applied electric field. The resulting fluid motion can be determined by solving the Navier-Stokes equation with the electrothermal body force.

Electro-osmotic flow (EOF) is most commonly associated with dc electric fields that are applied tangentially to a charged surface. Under static conditions, charge surfaces attract counter ions in the fluid forming a diffuse double layer of charge near the surface (Probstein, 1994). The tangential electric field produces a Coulomb force on the charge in the double layer, which viscously couples to the fluid, thereby inducing motion. A similar effect can occur with non-uniform ac electric fields. In this situation, the charged double layer is created by the normal component of the electric field and the Coulomb force by the tangent component of the electric field. Even though the tangential component is typically three or more orders of magnitude smaller than the normal component of the electric field, the net charge density in the double layer produces EOF.

Micron-resolution particle image velocimetry ( $\mu$ -PIV) can be used to measure detailed velocity fields in microfluidic devices with order one-micron spatial resolution. In PIV, fluid velocities are estimated by measuring the motion of flow-tracing particles in the fluid. It is assumed that the flow-tracing particles closely follow the flow. However, if electrophoretic or dielectrophoretic forces are significant, this assumption may not be valid. Therefore, electrical and viscous forces on the particles must be considered, to determine particle fidelity, and to estimate the underlying flow field. We extend the work of Meinhart & Wang (2001) by measuring particle motion using two different size particles, to account for the particle slip velocity resulting from DEP drift, and uniquely determine the fluid velocity.

---

\*Corresponding author.

## 2. Dielectrophoresis and Electrothermal Effect

### 2.1. Dielectrophoresis (DEP)

Dielectrophoresis induces particle movement in the direction of the gradient of the electric field intensity. This phenomenon occurs when the complex permittivity of the suspended particle differs from the fluid medium. Because of the small scales associated with microfluidic devices, DEP is particularly useful for separation of cells and macromolecules. DEP has been used to separate blood cells, cancer cells, bacteria, and to capture DNA molecules (Becker et al., 1994; Miles et al., 1999; Wang et al., 1993, 1997, 1998; Washizu et al., 1994, 1995; Yang et al., 1999). A review of particle separation techniques using DEP is given by Gasoyne and Vykoukal (2002).

DEP results from the particle's polarizability relative to the suspending medium. Following Jones (1995), the time-averaged dielectrophoretic force on a particle is

$$\bar{F}_{DEP} = \frac{1}{2} V \alpha \nabla \bar{E}_{rms}^2, \quad (1)$$

where  $\alpha$  is the effective polarizability of the particle,  $V$  is the volume of the particle and  $\bar{E}$  is the electric vector field. For a homogeneous uncharged sphere, the effective polarizability is given by

$$\alpha = 3\epsilon_m \Re\{K\}, \quad (2)$$

where  $\Re\{K\}$  is the real part of the Clausius-Mossotti factor

$$K = \frac{\epsilon_p^* - \epsilon_m^*}{\epsilon_p^* + 2\epsilon_m^*}. \quad (3)$$

The complex permittivities of the particle and the medium  $\epsilon_p^*$  and  $\epsilon_m^*$ , are defined as

$$\epsilon^* = \epsilon - j \left( \frac{\sigma}{\omega} \right), \quad (4)$$

where  $j = \sqrt{-1}$ ,  $\epsilon$  is the permittivity,  $\sigma$  is the conductivity, and  $\omega$  is the angular frequency of the applied electric field.

Combining equations (1) and (2) gives the well-known expression for the dielectrophoretic force on a sphere (Jones, 1995)

$$\bar{F}_{DEP} = 2\pi\epsilon_m r^3 \Re\{K\} \nabla E_{rms}^2. \quad (5)$$

where  $r$  is the sphere radius.

The magnitude of the DEP force scales with  $\sim r^3$ , and is usually significant for particles on the order of one micron or larger. The real part of the Clausius-Mossotti factor,  $\Re\{K\}$ , determines the magnitude and directional sign of the DEP force. This factor is bounded between

$-0.5 < \Re\{K\} < 1.0$  and depends upon the electrical properties of the particle and medium, and upon the frequency of the applied electric field. Positive DEP is defined when the DEP force vectors point towards increasing electric field intensity, which occurs for positive values of  $\Re\{K\}$ .

### 2.2. Electrothermal effect

The high intensity ac electric fields associated with dielectrophoresis can create non-uniform temperature fields. Permittivity and conductivity are often functions of temperature. Therefore, the spatially varying temperature fields create spatially varying permittivity and conductivity fields in the fluid. An applied electric field, coupled with spatial variations in permittivity and conductivity, creates non-uniform Coulomb and dielectric body forces in the fluid. This phenomenon is known as the electrothermal effect, and can induce microscale fluid motion, thereby non-invasively stirring the fluid at the microscale.

Following Ramos et al. (1998), the power per unit volume of the electrical field that is absorbed by the fluid due to Joule heating is given by

$$W = \sigma E^2. \quad (6)$$

The temperature of the fluid can be calculated by solving the heat equation with a source term for electrical heat generation

$$\rho_m c_p \left( \frac{\partial T}{\partial t} + \vec{u} \cdot \nabla T \right) = k \nabla^2 T + \sigma E^2, \quad (7)$$

where  $\vec{u}$  is the velocity,  $T$  is the temperature,  $\rho_m$  is the mass density,  $c_p$  is the specific heat (at constant pressure),  $k$  is the thermal conductivity, and  $\sigma$  is the electrical conductivity of the fluid medium.

For steady state conditions, and assuming the temperature advection is sufficiently small compared to conduction, equation (7) can be simplified

$$k \nabla^2 T + \sigma E^2 = 0. \quad (8)$$

By applying scaling arguments to equation (8), an order of magnitude estimate of the change in temperature in the medium can be estimated as

$$\Delta T \sim \frac{\sigma V^2}{k}, \quad (9)$$

where  $V$  is the applied voltage.

Gradients in temperature produce gradients in permittivity and conductivity in the fluid. For water  $(1/\sigma) (\partial\sigma/\partial T) = +2\%$  and  $(1/\epsilon) (\partial\epsilon/\partial T) = -0.4\%$  per degree Kelvin. These variations in electric properties produce gradients in charge density and perturbed the

electric field. Assuming the perturbed electric field is much smaller than the applied electric field, and that advection of electric charge is small compared to conduction, the time-averaged electrothermal force per unit volume for a non-dispersive fluid can be written as (Ramos et al., 1998)

$$\vec{f}_E = -0.5 \left[ \left( \frac{\nabla \sigma}{\sigma} - \frac{\nabla \varepsilon}{\varepsilon} \right) \cdot \bar{E}_0 \frac{\varepsilon \bar{E}_0}{1 + (\omega \tau)^2} + 0.5 |E_0|^2 \nabla \varepsilon \right], \quad (10)$$

where  $\tau = \varepsilon/\sigma$  is the charge relaxation time of the fluid medium. The first term on the right-hand side of equation (10) represents the Coulomb force, and the second term the dielectric force. At low frequencies,  $\omega\tau$ , the Coulomb force dominates. At high frequencies,  $\omega\tau$ , the dielectric force dominates. From Ramos et al. (1998), the two forces are equal in magnitude at the crossover frequency,  $\omega_c$ , where

$$\omega_c = 2\pi f_c \approx \frac{1}{\tau} \left( 2 \left| \frac{\partial \sigma}{\sigma \partial T} \right| / \left| \frac{\partial \varepsilon}{\varepsilon \partial T} \right| \right)^{1/2}. \quad (11)$$

Flows in microfluidic devices designed for molecular diagnostics typically have characteristic Reynolds numbers,  $Re = \rho_m u l / \eta$ , are typically lower than one. Therefore, the Navier-Stokes equation for steady state flow can be simplified to the Stokes' equation with a body force

$$\eta \nabla^2 \vec{u} - \nabla p + \vec{f} = 0, \quad (12)$$

and the mass-conservation equation for an incompressible fluid can be written as

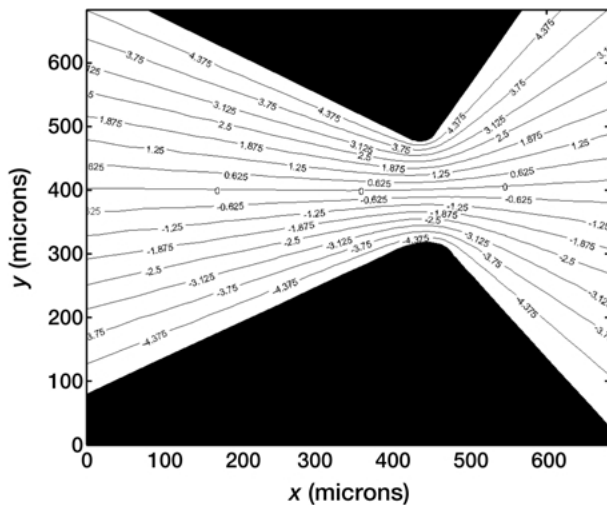


**Fig. 1.** Voltage potential of the DEP wedge device calculated using *Femlab*<sup>TM</sup> software.

$$\nabla \cdot \vec{u} = 0, \quad (13)$$

where  $\eta$  is the viscosity,  $p$  is the pressure and  $\vec{f}$  is the body force acting on the fluid. Using the no-slip boundary condition and setting the body force equal to the body force produced by the electric field, the fluid velocity resulting from the electrothermal effect can be determined.

### 3. Computer Simulations of the Electrothermal Flow

Figure 1 shows the instantaneous voltage potential of the basic wedge-shaped geometry. The black region represents two brass electrodes separated at the apex by approximately 200 microns. The voltage is calculated by solving  $\nabla^2 V = 0$ , using *Femlab*<sup>TM</sup> finite element software. The constant potential lines follow closely the contours of the electrodes. The electric field can be determined from the potential function. The dielectrophoretic force can be estimated by calculating the gradient of the electric field intensity

$$\vec{E} = -\nabla V, \quad (14)$$

and

$$F_{\text{DEP}} \sim \nabla E^2 = \nabla (\vec{E} \cdot \vec{E}). \quad (15)$$

Figure 2 shows the expected DEP force for negative DEP. The DEP force field points away from electrode gap and would tend to push the particles away from the electrode apex. Fluid motion is simulated by solving the

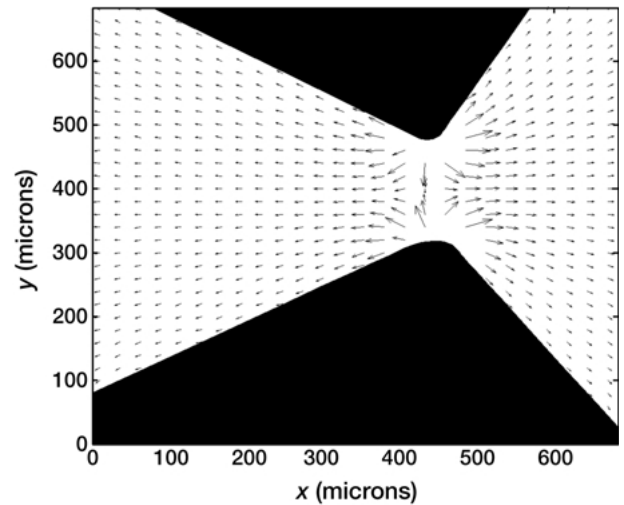


**Fig. 2.** Negative gradient of the electric field intensity, calculated using *Femlab*<sup>TM</sup> software. The vectors depict to within a constant the negative DEP force field.

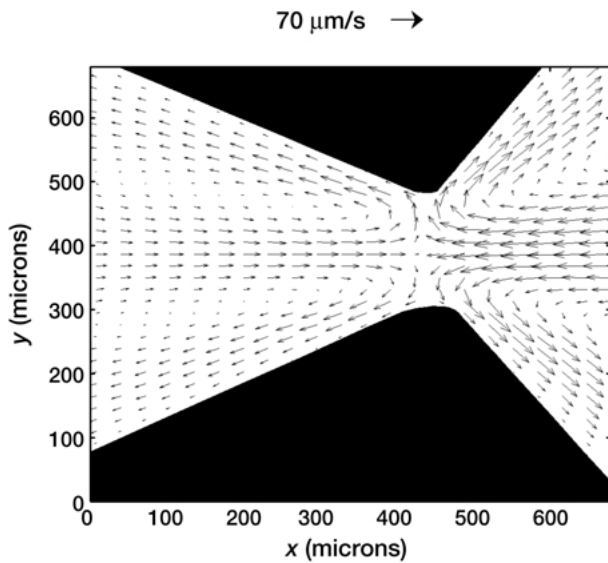


**Fig. 3.** Velocity field of the 1- $\mu\text{m}$  diameter particles in a fluid moving as a result of electrothermal forces and dielectrophoresis (estimated using Femlab<sup>TM</sup> software).

Stokes' equation, subject to the electrothermal effect. The velocity of particles relative to the fluid medium can be estimated by balancing the two dominant particle forces, Stokes' drag force and DEP force. The velocity field of a 1- $\mu\text{m}$  diameter particle, with a Clausius-Mossotti factor  $\Re\{K\} = -0.5$ , is shown in Figure 3. The particle velocity pattern shown in Figure 3 is significantly different from the force field shown in Figure 2, and suggests that in this configuration, these two phenomena have drastically different influences on particle motion.

#### 4. Micro-Resolution PIV Measurements

The recent development of micron-resolution Particle Image Velocimetry ( $\mu$ -PIV) has made possible the measurement of detailed fluid motion at the microscale, see Santiago et al. (1998) and Meinhart et al. (1999). Figure 4 shows a schematic of the micro-PIV system. The microfluidic device is placed just above the microscope objective lens. Fluorescently-dyed flow-tracing particles are suspended in a transparent working fluid inside a microfluidic device. Light from a Mercury arc lamp is passed through an excitation filter and relayed through a microscope objective lens into a microfluidic device. The illumination light excites the fluorescently dyed flow tracing polystyrene particles. Fluorescent light is emitted by the particles and imaged by the objective lens. The light passes through a fluorescent barrier filter, and is imaged onto a  $1,280 \times 1,024 \times 12$ -bit Hamamatsu CCD camera.

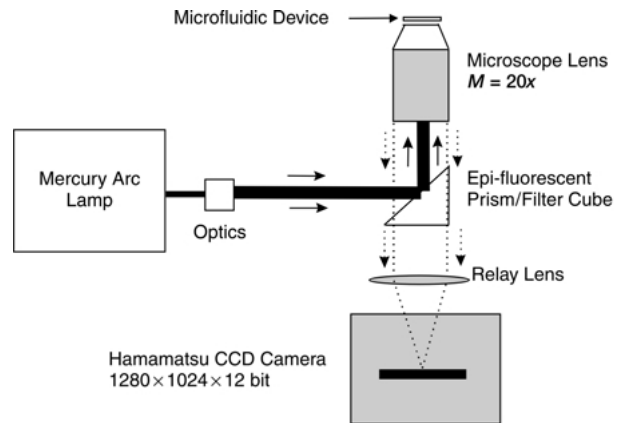


**Fig. 4.** Schematic of a micro-PIV system. A pulsed Nd:YAG laser is used to illuminate 200 nm diameter fluorescent flow-tracing particles through an epi-fluorescent inverted microscope. A cooled  $1,300 \times 1,030$  pixel  $\times$  12 bit interline-transfer CCD camera is used to record the particle images.

A series of 40 image fields were acquired at a rate of 13 frames per second. The image fields were subdivided into interrogation spots and cross correlated to determine the most probable displacement. At each interrogation spot, the time series of correlation functions were time-averaged to increase the signal-to-noise ratio, and avoid erroneous velocity data (see Meinhart et al., 2000).

The test section consists of two 100- $\mu\text{m}$  thick brass electrodes separated by approximately 200  $\mu\text{m}$  and sandwiched between two glass wafers. PIV measurements were obtained in the center of the device, at a depth of 50-microns. One-micron diameter polystyrene beads were suspended in an 8.5% (w/v) sucrose and 0.3% (w/v) dextrose sugar solution. A voltage potential was applied, with an amplitude of 10  $V_{\text{rms}}$  and a frequency  $f = 10$  kHz. For this experiment, the Clausius-Mossotti factor was  $K = -0.5$ . Therefore polystyrene particles exhibit negative dielectrophoresis.

Figure 5 shows the velocity field of 1- $\mu\text{m}$  diameter particles. The velocity vectors indicate that the particle flow pattern recirculates. In the middle of the device, the particles are drawn towards the apex of the electrodes where a stagnation point exists. Near the device center, the particles turn toward the outside and are pushed along the electrodes and away from the center.

The actual motion of the polystyrene particles measured experimentally using micro-PIV shown in Figure 5 is not consistent with the DEP force field pattern shown in Figure 2. Therefore, we concluded that DEP forces are not the dominant mechanism. However, the particle velocity field resulting from solving Stokes equation with electrothermal forcing is shown in Figure 3. The flow pattern closely resembles that of the experimental measurements shown in Figure 5, except

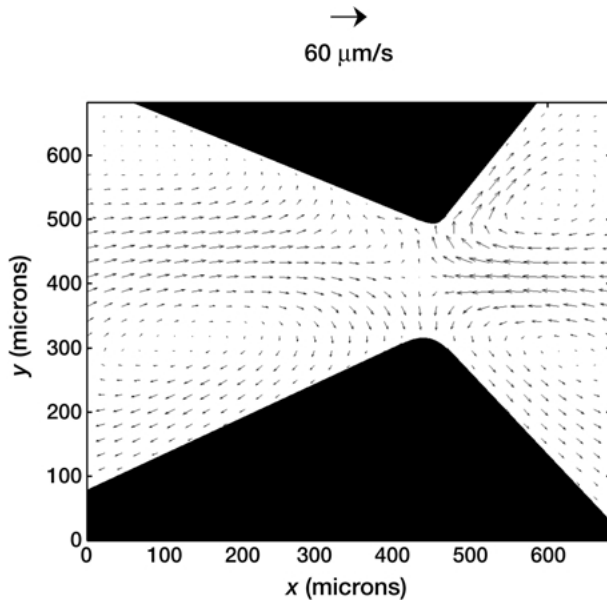


**Fig. 5.** Micron-resolution PIV velocity field of 1- $\mu\text{m}$  diameter polystyrene particles under the influence of dielectrophoresis and viscous coupling to the fluid motion. The motion is similar to what one would expect with electrothermally-driven flow.

the velocity scale is approximately  $60 \mu\text{m/s}$  for the PIV results, and  $70 \mu\text{m/s}$  for the electrothermal simulation.

Due to negative DEP forces acting on the polystyrene particles, the particles may not follow the flow faithfully. The particle slip velocity due to DEP forces can be estimated by balancing Stokes drag with the DEP force for non-accelerating particles

$$\vec{F}_{DEP} + \vec{F}_D = 0. \quad (16)$$

Combining equations (5) and (16) and rearranging yields the particle velocity  $\vec{u}_p$  relative to the fluid velocity  $\vec{u}$ .

$$\vec{u}_p - \vec{u} = \frac{\epsilon_m r^2 \Re\{K\} \nabla E_{rms}^2}{3\mu}. \quad (17)$$

Solving equation (17) requires knowledge of the dielectric and conductivity properties of the fluid and particle to estimate the Clausius-Mossotti factor,  $K$ , and an estimation of the gradient of the electric field. In microfluidic devices, it is difficult to measure the electric field accurately. Therefore, one must rely on numerical simulations to calculate the electric field.

The fluid velocity can be measured by performing two separate micro-PIV experiments using two different size particles, but with similar electrical properties. Since  $F_{DEP}$  scales with  $r^3$  and  $F_D$  scales linearly with  $r$ , we can uniquely solve for fluid velocity by comparing the two velocity fields measured from the two different size particles

$$\vec{u} = \frac{\vec{u}_{p1} r_2^2 - \vec{u}_{p2} r_1^2}{r_2^2 - r_1^2}, \quad (18)$$

where  $\vec{u}_{p1}$  and  $\vec{u}_{p2}$  are the particle velocity fields, and  $r_1$  and  $r_2$  are the particle radii from experiments 1 and 2, respectively.

A wedge-shaped test section was micromachined from a  $550\text{-}\mu\text{m}$  thick silicon wafer. The test section fabrication is a three-step process consisting of photolithography, deep reactive ion etching and metal deposition. A  $3\text{-}\mu\text{m}$  thick layer of  $\text{SiO}_2$  was deposited on a silicon wafer by PECVD. During lithography, SPR510A photoresist was coated and exposed beneath a mask containing the channel pattern with a 6300B DSW Wafer Stepper. After development the wafer was soaked in BHF for 6 minutes to etch off exposed  $\text{SiO}_2$ . The wafer was etched through using Deep RIE, which took approximately 5 hours. Metal electrodes,  $500 \text{ \AA}$  Ni and  $2,000 \text{ \AA}$  Au, were deposited using an e-beam evaporator, which provided good sidewall coverage. Finally, the wafer was cut with Disco Dicing Saw and the resulting chip was sandwiched between two glass wafers to form the microfluidic device (see Figure 6).

The test section was filled with an aqueous solution consisting of 8.5% (w/v) sucrose and 0.3% (w/v) dextrose sugar. Sugar was added to eliminate electrolysis for low frequency electric fields. An external voltage of  $20 \text{ V}_{rms}$  was applied at a frequency  $f = 100 \text{ kHz}$ . The Clausius-Mossotti factor for polystyrene particles at this frequency was  $\Re\{K\} = -0.5$ . Two PIV experiments were performed at a depth of 40-microns from the top glass wafer. One-micron and two-micron diameter particles were used. The particle velocity fields are shown in Figures 7 and 8.

Since the particle velocity fields of two similar particles of different size is known, equation (18) can be used to estimate the underlying fluid velocity, without any knowledge of the electrical properties of the particles. This estimate of fluid velocity is shown in Figure 9. The characteristic velocity is  $110 \mu\text{m/s}$ , which

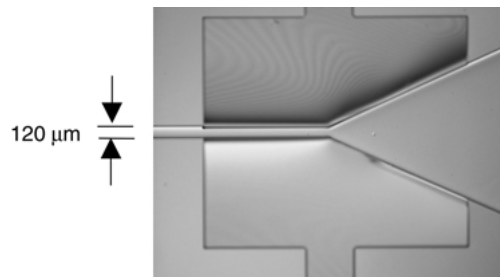


**Fig. 6.** Picture of a precision microfabricated wedge-shaped device. The  $550 \mu\text{m}$  thick channel is formed by Deep RIE a silicon wafer, and using e-beam deposition to deposit Ni and Au electrodes. The channel width is  $120 \mu\text{m}$ .

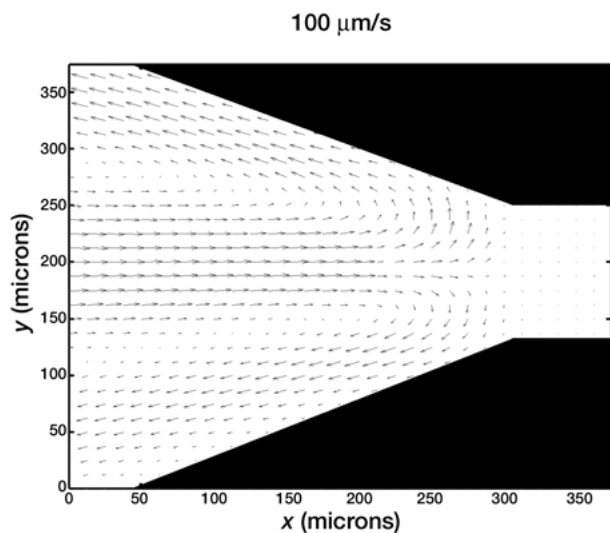


**Fig. 7.** Particle velocity field of 1- $\mu\text{m}$  diameter polystyrene particles. The maximum velocity at the center line is approximately 100  $\mu\text{m/s}$ .

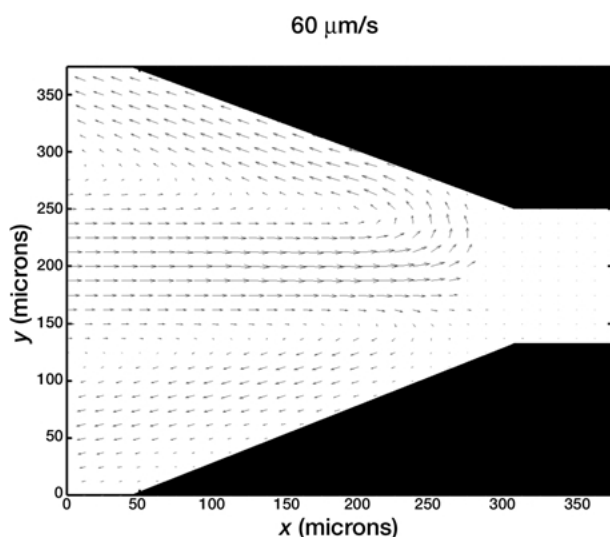


**Fig. 8.** Particle velocity field of 2- $\mu\text{m}$  diameter polystyrene particles. The maximum center line velocity is approximately 40  $\mu\text{m/s}$ .

is about 10% higher than the 1- $\mu\text{m}$  diameter particle velocity (Figure 7). It is also qualitatively similar to the electrothermally-driven flows shown in Figures 3 and 5.

## 5. Conclusion

Micron-resolution particle image velocimetry ( $\mu$ -PIV) is used to measure accurately trajectories of polystyrene particles under the influence of an applied ac electric field. The PIV results of 1- $\mu\text{m}$  diameter particles agree qualitatively with computer simulations of particle

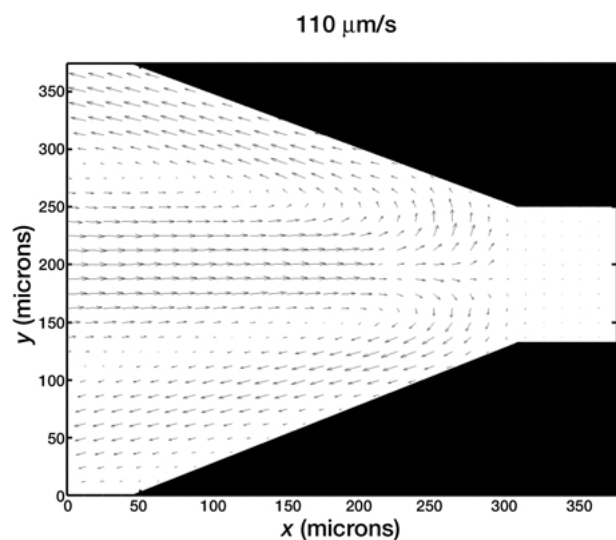


**Fig. 9.** Fluid velocity field estimated using PIV data measured with 1- $\mu\text{m}$  and 2- $\mu\text{m}$  diameter particles and equation (18). The minimum width between the electrodes is 120  $\mu\text{m}$ . The applied voltage is 20  $V_{\text{rms}}$  at a frequency of  $f=100$  kHz. The characteristic velocity is 110  $\mu\text{m/s}$ .

motion resulting from electrothermal forces near the electrodes. For the experimental parameters considered here, with applied electric field frequencies of  $f=10$  and 100 kHz, the electrothermal forces appear significant compared to the DEP forces. A micro-PIV experiment was conducted using similar particles, with 1- $\mu\text{m}$  and 2- $\mu\text{m}$  diameters. The particle velocity fields were used to uniquely estimate fluid motion, independent of the electrical properties of the particles and the medium, and the underlying electric field. The estimate of fluid velocity in the center of the flow cell is approximately 10% higher than the velocity of the 1- $\mu\text{m}$  diameter particles.

## Acknowledgments

This work is supported by DARPA/ARMY DAAD 19-00-1-0400, DARPA/Air Force F30602-00-2-0609, NSF CTS-9874839, and NSF ACI-0086061.

## References

- F.F. Becker, X.-B. Wang, Y. Huang, R. Pethig, J. Vykoukal, and P.R. Gascoyne, *Journal of Physics D: Applied Physics* **27**(12), 2659–2662 (1994).
- P.R.C. Gascoyne and J. Vykoukal, *Electrophoresis* **23**, 1973–1983 (2002).
- T. Jones, *Electromechanics of Particles* (Cambridge University Press, New York, NY, 1995).

- C.D. Meinhart, S.T. Wereley, and J.G. Santiago, *Exp. in Fluids* **27**, 414–419 (1999).
- C.D. Meinhart, S.T. Wereley and J.G. Santiago, *J. Fluids Eng.* **122**, 285–289 (2000).
- C.D. Meinhart and D. Wang, *Proceedings of  $\mu$ -TAS*, Monterrey, CA, 2001.
- R. Miles, P. Belgrader, K. Bettencourt, J. Hamilton, and S. Nasarabadi, *Proceedings of the ASME International Mechanical Engineering Congress and Exposition* (November 14–19, Nashville, TN, 1999).
- R. Probstein, *Physicochemical Hydrodynamics*, 2nd edn (Wiley, New York, 1994).
- A. Ramos, H. Morgan, N.G. Green, and A. Castellanos, *J. Phys. D: Appl. Phys.* **31**, 2338–2353 (1998).
- J.G. Santiago, S. Wereley, C.D. Meinhart, D.J. Beebe, and R.J. Adrian, *Exp. Fluids* **25**(4), 316–319 (1998).
- X.-B. Wang, Y. Huang, J.P.H. Burt, G.H. Markx, and R. Pethig, *J. Phys. D: Appl. Phys.* 1278–1285 (1993).
- X.-B. Wang, Y. Huang, X. Wang, F.F. Becker, and P.R. Gascoyne, *Biophys. J.* **72**, 1887–1899 (1997).
- X.-B. Wang, J. Vykoukal, F. Becker, and P. Gascoyne, *Biophys. J.* **74**, 2689–2701 (1998).
- M. Washizu, S. Suzuki, O. Kurosawa, T. Nishizaka, and T. Shinohara, *IEEE Transactions on Industry Applications* **30**(4), 835–842 (1994).
- M. Washizu, O. Kurosawa, I. Arai, S. Suzuki, and N. Shimamoto, *IEEE Transactions on Industry Applications* **32**(3), 447–445 (1995).
- J. Yang, Y. Huang, X. Wang, X.-B. Wang, F. Becker, and P. Gascoyne, *Biophys. J.* **76**, 3307–3314 (1999).